Reprint 1524

Enhancement of the HKO Satellite Derived Radar Reflectivity Algorithm in Recognition of Significant Convection

CHAN Wai-soen, Christy LEUNG Yan-yu and LI Ping-wah

The 34th Guangdong - Hong Kong - Macao Seminar
on Meteorological Science and Technology
and
The 26th Guangdong - Hong Kong - Macao Meeting
on Cooperation in Meteorological Operations

(Macau 3-5 November 2021)

Intellectual Property Rights Notice

Disclaimer

天文台卫星模拟雷达反射率强对流识别加强版算法

陈维洵 梁恩瑜 李炳华

香港天文台

摘要

香港天文台于 2017 年开发了一套利用机器学习技术的卫星反演雷达反射率算法，利用日本气象厅向日葵 8 号地球同步气象卫星收集的数据，配合地面雷达反射率，模拟大范围的雷达反射率。这种从卫星反演的雷达反射率，由于具有大覆盖范围及高频率更新的优点，是香港天文台进行强对流临近预报的其中一个重要工具。本文介绍一个反演算法的增强版本，用以提高识别强对流的表现。本文并以全国雷达拼图验证卫星反演雷达反射率。结果显示改善了的演算法，较原有的演算法更能识别强对流。本文亦讨论有关这个演算法的下一步发展工作。

Enhancement of the HKO Satellite Derived Radar Reflectivity Algorithm in Recognition of Significant Convection

Wai-soen Chan, Christy Yan-yu Leung and Ping-wah Li

Hong Kong Observatory

Abstract

The Hong Kong Observatory developed a satellite reflectivity retrieval algorithm using machine learning technique in 2017 to simulate large area "radar reflectivity" by matching Japan Meteorological Agency's Himawari-8 geostationary meteorological satellite data with surface weather radar data. This satellite derived radar reflectivity, covering a large geographical domain and updated at high frequency, is one of the main tools for significant convection nowcast at the Observatory. This paper presents several enhancements to the existing retrieval algorithm to improve its performance in recognizing significant convection. The paper also presents the verification results of the new algorithm by comparing the retrieved reflectivity against national radar mosaic. The results indicate an improvement in the skill of the new algorithm over the existing algorithm. The paper will also discuss the future development work on the retrieval algorithm.

1. Introduction

The Hong Kong Observatory (HKO) developed a satellite reflectivity retrieval algorithm using machine learning technique in 2017 to simulate large area "radar reflectivity" by matching Japan Meteorological Agency's Himawari-8 (H-8) geostationary meteorological satellite Advanced Himawari Imager (AHI) data with surface weather radar data [1-2]. Given the positive skill in significant convection identification, the algorithm was deployed as a part of the thunderstorm nowcast module of a web platform to support forecasters from different Meteorological Watch Offices (MWOs) in the Asia Pacific (APAC) region to issue WS (thunderstorm) SIGMET [3].

Since the users of the web platform spanned a large geographical area over the APAC region, several enhancements of the satellite derived radar reflectivity algorithm from [1-2] were required to adapt to the variability over the domain. This paper highlights several enhancements to the existing retrieval algorithm to improve the performance in recognizing significant convection. Moreover, the application of the derived radar reflectivity on thunderstorm nowcast would also be discussed. The paper will also discuss the future development work on the retrieval algorithm.

2. The Algorithm and its Enhancement

Machine Learning Model

Similar to the previous study [1,3], we employed the multilayer perceptron (MLP) as our machine learning model, to predict the reflectivity at each satellite pixel. There are a couple of benefits in using the MLP, first the MLP is non-linear activating, which can handle the non-linearity of the relationship between the predictors and the predictands. Radar reflectivity and brightness temperatures measured by satellite are related through complicated physical processes that could be handled only by non-linear models. Secondly, since the MLP could be applied to different pixels independently, we can expand the training dataset by concatenating the data.

Input predictors

The previous study [1,3] had discussed the choice of input predictors in the development of the artificial neural network (ANN) model. In this section we discuss the enhancement being made. The enhanced model consists of two separated ANN networks, one made use of 7 channels of the H-8 AHI which consisted of 3 visible/near infrared albedos and 4 far infrared brightness temperatures as input. The other network made use of the same 4 channels of far infrared brightness temperatures. The albedos of the 3 visible/near infrared channels were preprocessed before feeding into the model. Details could be found in the Section *Preprocessing of input data* below. Table 1 summarizes the channels and input parameters used in the enhanced model. Similar to previous finding, the model involving visible/near infrared channels performed better than the model using only the far infrared channels. However, due to the availability of the visible and near infrared channels over nighttime, both networks were used in the enhanced algorithm to provide all-day derived reflectivity. The output of reflectivity was obtained by taken a weighted mean of the two outputs, when available, to ensure continuity in space and time. The weighting was related to sunlight availability at each pixel according to the solar elevation angle at each grid point.

The previous study had incorporated a seasonal parameter, day-of-the-year, to mimic any seasonal variability. This choice of seasonal parameter was suitable in their study because the domain was in the vicinity of Hong Kong. However, in the current study, since the target area of service spanned the northern and southern hemisphere, such parameter would not be appropriate. Instead, we made use of the solar elevation angle, at noon of each local point of the day, to take care of the seasonal effect.

Apart from the seasonal parameter, two other parameters, namely the solar location parameter and satellite location parameter were added into the Night Mode. The addition of these two parameters was to take into account any variability of measured brightness temperatures, due to geometric difference of satellite and the sun, across the pixels. For Day Mode, as described below, an independent treatment of the albedos was carried out and hence they were not put into the model as predictors.

	Night Mode	Day Mode
Predictors	• Brightness temperatures of B08, B10, B13, and B15[1] • Seasonal parameter • Solar location parameter • Satellite location parameter	• Calibrated albedos of B03, B04, and B05 • Brightness temperatures of B08, B10, B13, and B15 • Seasonal parameter
Predictand	Radar Reflectivity	

Table 1. The predictors and predictand of the ANNs

Preprocessing of input data

To take into account the solar effect, the visible and near infrared satellite data were pre-processed before feeding into the model. Since the predictors were measured by a geostationary satellite located at a fixed point relative to Earth surface, the viewing angle of the satellite, as well as the position of the Sun, could bring bias to the measurement at different places due to optical processes such as reflection and attenuation. These effects should not be ignored. The pre-processing of predictors before feeding into the model could regularize the data from location variations that is not delineated by the predictors and allow concatenating the data from different pixels in training the model.

In radiative transfer, for visible and near infrared albedos, the location variation could be described by the reflection process and Rayleigh scattering of sunlight by the atmosphere. The radiance of each pixel measured by satellite depended on a few quantities, including the variation of solar radiance due to the periodic change of Sun-Earth separation in the elliptical orbit of Earth and the optical path of the sunlight entering the atmosphere and reflected by the

[1] Definition of channels in Himawari 8 AHI could be found at JMA's website: https://www.data.jma.go.jp/mscweb/en/himawari89/space_segment/spsg_ahi.html

clouds. The corrected albedo $\tilde{A}$ is therefore given by

$$\tilde{A} = \frac{1}{t(\theta_{\mathrm{sat}}, \theta_{\mathrm{sol}}) \cos\theta_{\mathrm{sol}}} \left(\frac{r}{1\ \mathrm{AU}}\right)^2 \frac{\pi I}{S_0} \qquad ,$$

where I is the measured radiance, S_0 is the band solar irradiance [4], r is the Sun-Earth separation, θ_{sol} is the solar zenith angle, θ_{sat} is the satellite zenith angle, and t is the attenuation correction function due to Rayleigh scattering [5,6], which depends on optical path and hence solar zenith angle, satellite zenith angle, and the location of the pixel. The attenuation correction term was obtained using an empirical formula of Rayleigh scattering under standard atmosphere [6]. Figure 1 shows the result of the calibrated visible channel image. Employing a physical formulation has an advantage over statistical approach when calibrating the image because the physical feature of the cloud top could be preserved. Although the calibration could be carried out to all pixels in principle, the visible/near infrared data at pixels with sun elevation less than 20 degrees would not be used, since the reflection of sun light at such small elevation angle would be mainly by the lateral of the clouds.

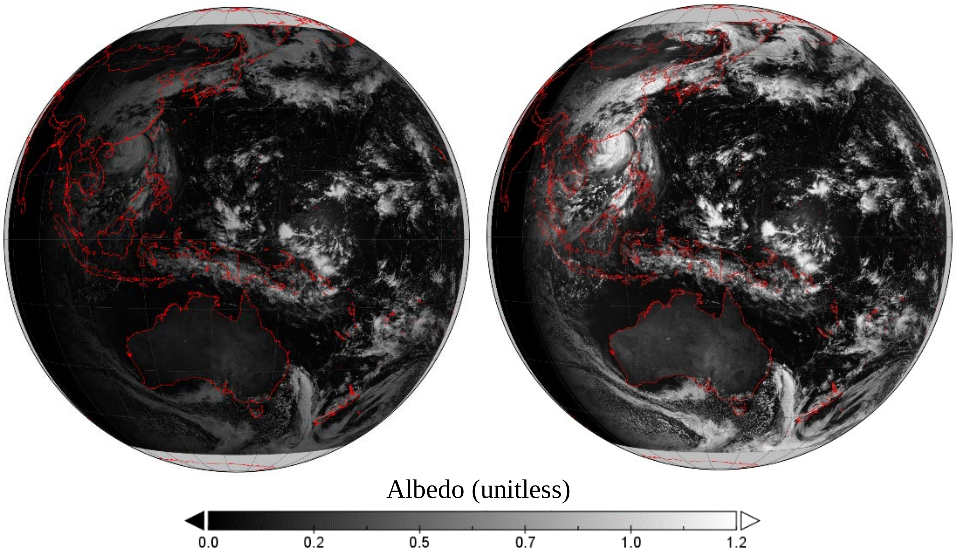

Figure 1. Sample H-8 B03 (0.639 μm) imagery taken on 16 September 2018 00:00 UTC. Left: before preprocessing, right: after preprocessing. The preprocessing would regularize the satellite measurements at different places due to optical process, which could remove bias during model training.

Training dataset

Since the area of coverage of the satellite image extends from southern to northern hemisphere, and from eastern Indian Ocean to the central Pacific, the climatology and characteristics of convections vary from region to region over the pixels. To accommodate the behavior of convections at different locations, the training dataset was expanded from solely HKO radar data to also include the China Meteorological Administration (CMA) national radar mosaic composite reflectivity. Composite reflectivity was chosen to train the model because it could better represent the vertical structure of convections, in comparison with satellite imageries, which mostly represent the upper part of the atmospheric column.

In this study, we have incorporated a dataset of three months, i.e. August, September and December of 2018. For matching satellite and radar data, observations measured at 00-minute and 30-minute were use (since radar volume scan updated in every 6 mins while satellite scan updated in every 10 mins). To segregate the data into (i) training and (ii) validation sets, data at odd hours were used for training while even hours were used for verification. For Day Mode, data at 01, 03, and 05 UTC were used while for Night Mode, data from the whole day were used.

Verification of the enhanced algorithm

The satellite derived radar reflectivity field was verified against the national radar mosaic. Figure 2 shows the Receiver Operating Characteristic (ROC) curve of the existing and enhanced algorithm of the satellite derived radar reflectivity. It is evident that for convection above 20 dBZ, the enhanced algorithm performed better than the existing version. Figure 3 shows an example of the comparison of the derived reflectivity fields using the existing and enhanced algorithm, with actual radar measurement and the satellite deep convection image (IR1 – IR3) at the same time as reference. The comparison again shows that the enhanced algorithm could better capture the shape and intensity of the convective regions better than the existing algorithm.

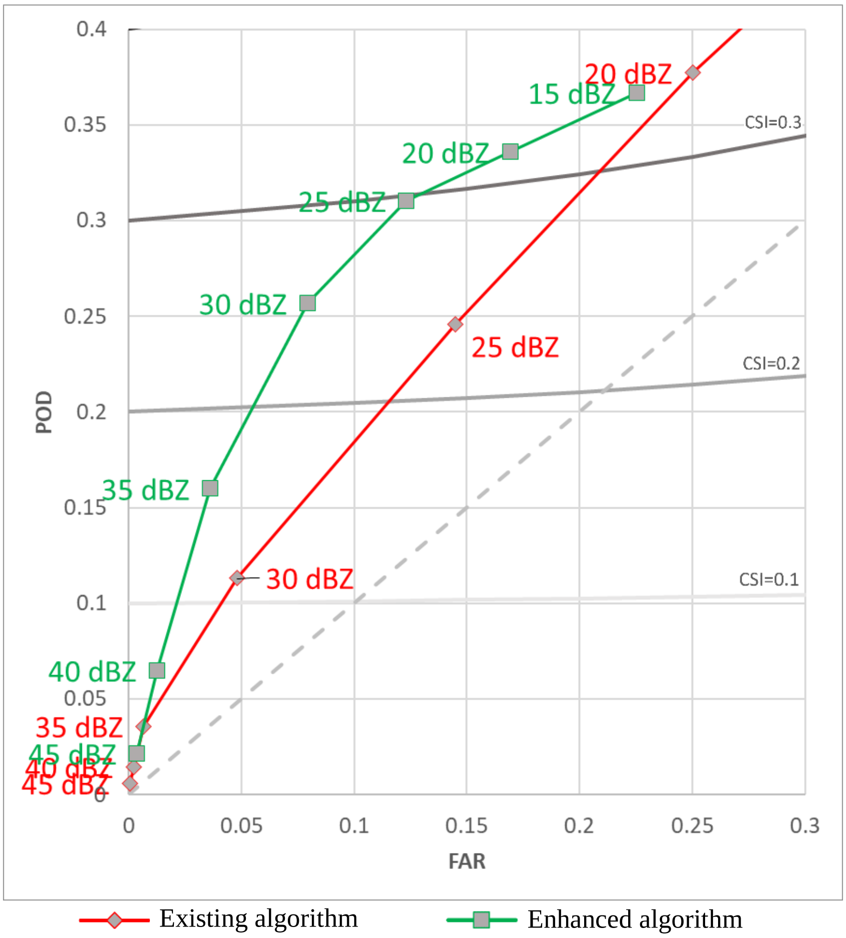

Figure 2. Performance of the existing and enhanced algorithms for satellite derived radar reflectivity.

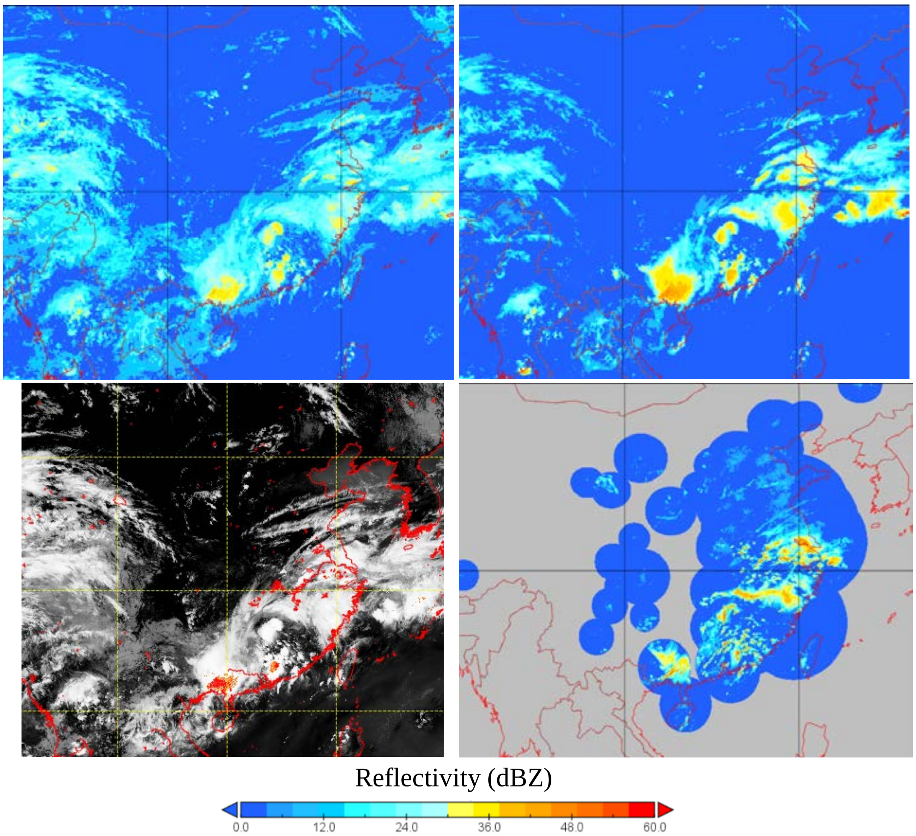

Figure 3. A case on 5 June 2020 05:00 UTC. Top left: existing satellite derived radar reflectivity, top right: enhanced satellite derived radar reflectivity. Bottom left: deep convection satellite imagery of H-8, red areas represent regions with deep convection. Bottom right: CMA National Radar Mosaic

3. Application in Convection Identification and Thunderstorm Nowcast

One obvious advantage of geostationary satellite observation over radar in monitoring convection is the greater spatial coverage. With the analysis field of convection updated every 10 minutes, nowcasting convective activities using optical flow and semi-Lagrangian advection scheme (similar to [7-9]) were carried out. Figure 4 shows an example of convective nowcast product using the enhanced satellite derived radar reflectivity combined with global lightning data. This nowcast product could provide reference to aviation forecasters of different MWOs in the APAC region for monitoring and issuance of hazardous weather warnings in association with significant convections.

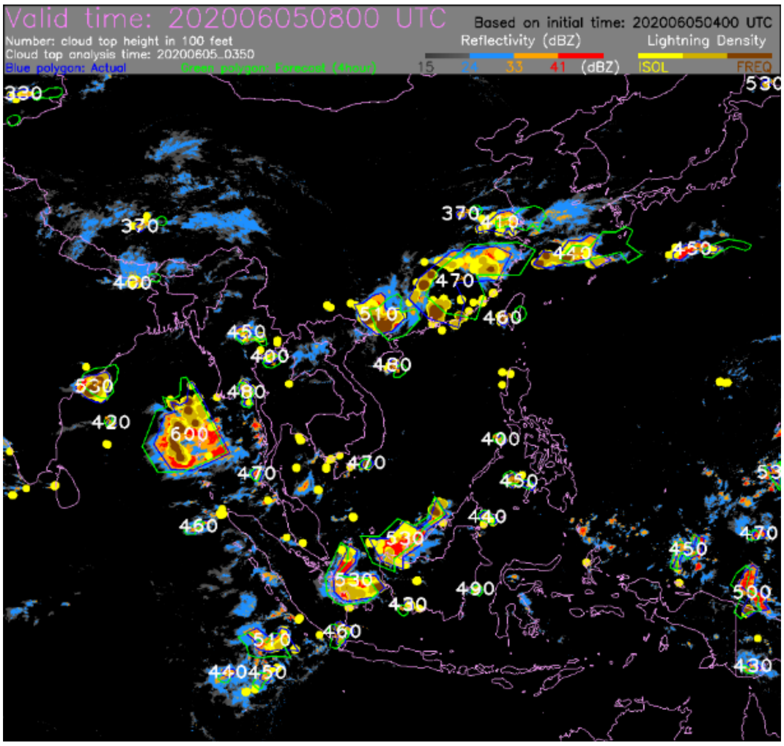

Figure 4. The 4-hour convective nowcast product using the enhanced satellite derived radar reflectivity, combined with global lightning data. White numbers represent cloud top height [3].

4. Future Work

Apart from calibration on visible and near infrared channels, the measured radiance of far infrared channels also suffered from attenuation. The attenuation is due to absorption by the atmospheric trace gases along the optical path such as water vapour and ozone. The measured radiance by satellite at a larger view angle is normally weaker than those at smaller view angle and as a result the derived brightness temperature would appear cooler closer to the edge than the centre of the satellite image. This effect is known as limb cooling. Recent efforts [10,11] attempted to correct the limb cooling effect using a semi-physical approach by establishing the limb correction using the brightness temperature from satellite against the one derived from the radiative transfer model on trace gases from model re-analysis data. The correction was then fit with an empirical formula as a function of satellite zenith angle. Further efforts would be spent to explore the benefits of the inclusion of the correction of limb cooling in the algorithm.

The current training dataset covered from sub-tropics to mid-latitudes. The satellite derived radar reflectivity would be best behaved over these regions. However, it was known that the convective activities near the ITCZ are more frequent and violent, and more likely to contain solid hydrometeor, which would give a much larger reflectivity values as measured by radar. Further efforts may need to be spent on exploring the analysis of convection intensities using satellite observations over the equatorial area.

Lastly but not least, various satellite channels could also be simulated by incorporating high resolution NWP model outputs into radiative transfer model. Depending on the resolution of the NWP system, these simulated satellite images could be of high quality, which could be treated as an input and applied to the current MLP model to give forecast images of satellite derived radar reflectivity.

Acknowledgements

The authors would like to thank Ms S.Y. Lau for her valuable comments on the research project and this report.

Reference

[1] Woo, W. C., Ip, Y. Y., Wong, W. K. & Chan, N. H. (2017). Development of Satellite Reflectivity Retrieval Technique for Tropical Cyclone Rainfall Nowcasting. *Fourth International Workshop on Tropical Cyclones Landfall Processes* (IWTCLP-4), Macau, China, 5-7 December 2017

[2] Woo, W. C., Chan, N. H., Ip, Y. Y., & Wong, W. K. (in press). Equivalent Radar Reflectivity Derived from Advanced Himawari-8 Imager Data using Artificial Neural Network.

[3] Leung, C. Y. Y., Tam, H. C., Chan, W. S., & Fok, H. K. (2020). Development of satellite-based cloud top height and convection nowcasting products in support of SIGMET coordination in APAC region. *100th American Meteorological Society Annual Meeting*, Boston, U.S.A., 12–16 January 2020

[4] Japan Meteorological Agency (2005). Himawari-8/9 Himawari Standard Data User's Guide. Retrieved from https://www.data.jma.go.jp/mscweb/en/himawari89/space_segment/hsd_sample/HS_D_users_guide_en_v12.pdf

[5] Kasten, F. (1965). A new table and approximation formula for the relative optical air mass. *Archiv für Meteorologie, Geophysik und Bioklimatologie, Serie B*, *14*(2), 206-223.

[6] Kasten, F., & Young, A. T. (1989). Revised optical air mass tables and approximation formula. *Applied Optics*, *28*(22), 4735-4738.

[7] Wong, W.K., Yeung, L.H.Y., Wang, Y.C., & Chen, M. (2009). Towards the Blending of NWP with Nowcast — Operation Experience in B08FDP. *WMO Symposium on Nowcasting*, 30 Aug - 4 Sep 2009, Whistler, B.C., Canada

[8] Yeung, L.H.Y., Wong, W.K., Chan, P.K.Y., & Lai, E.S.T. (2009). Applications of the Hong Kong Observatory nowcasting system SWIRLS-2 in support of the 2008 Beijing Olympic Games. *WMO Symposium on Nowcasting*, 30 Aug-4 Sep 2009, Whistler, B.C., Canada.

[9] Cheung, P., & Yeung, H.Y. (2012). Application of optical-flow technique to significant convection nowcast for terminal areas in Hong Kong. In *The 3rd WMO International Symposium on Nowcasting and Very Short-Range Forecasting (WSN12)* (pp. 6-10).

[10] Elmer, N. J., Berndt, E., & Jedlovec, G. J. (2016). Limb correction of MODIS and VIIRS infrared channels for the improved interpretation of RGB composites. *Journal of Atmospheric and Oceanic Technology*, *33*(5), 1073-1087.

[11] Elmer, N. J., Berndt, E., Jedlovec, G., & Fuell, K. (2019). Limb Correction of Geostationary Infrared Imagery in Clear and Cloudy Regions to Improve Interpretation of RGB Composites for Real-Time Applications. *Journal of Atmospheric and Oceanic Technology*, *36*(8), 1675-1690.